JOM Journal of Optical Microsystems

RESEARCH PAPER

Combining Bragg reflector and Fabry–Pérot cavity into a solid-state electrochromic device for dynamic modulation

Jiacheng Hu,[a] Qingjiao Huang,[a] Wenshuai Feng,[a] Yongfeng Wang,[a] Menghan Yin,[a] Peipei Shao,[a] Bowen Li,[a] Ying Zhu,[a] and Rui-Tao Wen[a,b,*]

[a]Southern University of Science and Technology, Department of Materials Science and Engineering, Shenzhen, China

[b]Southern University of Science and Technology, Guangdong Provincial Key Laboratory of Functional Oxide Materials and Devices, Shenzhen, China

ABSTRACT. The dynamic color control of solid-state electrochromic (EC) devices has sparked broad interest in both academia and industry. In this work, we report a combination of an optical stack of a Bragg reflector and Fabry–Pérot cavity into a solid-state EC device that achieves high brightness and saturation. The Bragg reflector and Fabry–Pérot optical stacks are designed as multi-color selectors through dynamically varying the optical constants (***n*** and ***k***) of the EC layer, allowing selective reflection of different wavelengths. By employing EC-inactive mixed-tungsten-vanadium oxide as the counter electrode, high reflectivity and contrast can be ensured. The demonstrated combination of the Bragg reflector and Fabry–Pérot cavity into a solid-state EC device offers a practical approach to designing and fabricating high-performance reflective EC devices.

Keywords: multi-color; electrochromic device; Bragg reflector; F–P cavity

Paper 24003SS received Feb. 2, 2024; revised Apr. 11, 2024; accepted May 21, 2024; published Jun. 13, 2024.

1 Introduction

Electrochromic (EC) technology stands out as a highly innovative solution capable of dynamically adjusting the transmission, reflectance, and absorption of an object while maintaining a low energy consumption.[1] It has sparked extensive efforts and holds significant potential for various applications, such as smart windows, displays, sensors, and thermal regulation.[2–8] Solid-state EC devices are supposed to possess excellent cycling stability and resistance to solar radiation. However, inorganic metal oxides normally lack color saturation and gamut. Redel et al.[9] used the arrangement of materials of high (WO_3) and low (NiO) refractive indices to form a Bragg reflector in EC electrodes, which formed a noticeable structural color. The complementary coloring effect from the cathodic (WO_3) and anodic (NiO) EC materials limited the dynamic modulation range of reflectance. Xiao et al.[10] fabricated a Bragg reflector by regulating the glancing deposition angle of a single component oxide (WO_3) through electron-beam evaporation. The porosity of the deposited WO_3, which could vary the refractive index, was changed by adjusting the incident angle during deposition. This avoids conflict with the complementary coloring effect and enables the variation of structural colors with dynamic modulation. The Bragg reflector successfully achieved commendable color saturation; however, the structure of the device is complex since their Bragg reflector consisted of about 40 stacked layers. With subsequent layer

*Address all correspondence to Rui-Tao Wen, wenrt@sustech.edu.cn

incorporations, for example, the electrolyte, counter electrode and transparent conductive layers, the structure of the device becomes more complicated.

In addition, there are multi-color EC electrodes based on the Fabry–Pérot resonance. A configuration of a metal reflector layer (W) and an EC layer (WO_3) was employed to construct the Fabry–Pérot (F–P) cavity,[11,12] thereby engendering structural colors and notable multi-color variations. Nevertheless, the prospect of improving both the saturation and the color gamut remains extant. In EC devices, the sol-gel electrolyte is usually utilized, which introduces poor resistance to solar radiation compared with solid-state EC devices. Other attempts have also been made, for example, complementary color overlays formed in Co_3O_4 and Prussian blue,[13] and the attainable color space can be enriched to include green and brownish. The diverse structural color variation is promising in optical instruments, solar cells, nanophotonics, and photodetectors;[14–18] however, it is hard to achieve in the solid-state EC device in which the interference is taken as a "turbulence." In general, low brightness, poor saturation, and narrow gamut are the "stumbling blocks" for multicolor EC devices, and no satisfactory solution has been found to date.[6]

In this work, we report an approach to construct a simple structural configuration to achieve high brightness and color saturation in solid-state EC devices. Different from traditional designs, we combined a Bragg reflector, F–P cavity, and EC material within a single device. For the first time, the interference is taken as a positive factor to form the structural color in the EC device. The Bragg reflector is employed to achieve high color saturation, whereas the F–P cavity plays the role as a dynamic color modulator. The combination of the Bragg reflector and F–P cavity aims to form a focused absorption for high contrast without reducing the reflectance across the visible light range. Additionally, we utilized EC inactive material of mixed-tungsten-vanadium oxide (WVO) to prevent the reduction of brightness and saturation that is caused by excessive absorption during the lithium intercalation process. Li_3PO_4 (LPO) was selected as the electrolyte. As a demonstration, the Bragg reflector formed by ITO/WVO/LPO/WO_3 and the F–P cavities formed by WO_3/Cu were constructed. Due to the EC inactive nature of WVO upon ion intercalation, high reflectivity was maintained throughout the dynamic coloration process. Benefiting from these optical strategies, a solid-state EC device with a structure of glass/ITO/WVO/LPO/WO_3/Cu was demonstrated; it initially exhibited a grass-green color that can gradually change to dark brown.

2 Materials and Methods

2.1 Thin Film Deposition and Device Fabrication

The distance of the target-to-substrate was about 8 cm. Prior to deposition, the vacuum chamber was evacuated to $\sim 6 \times 10^{-4}$ Pa, and the target was pre-sputtered for 15 min in pure argon gas to remove surface oxides and other impurities. The substrate was rotated at a speed of 20 times per minute during the deposition process. After deposition, the samples were kept in the chamber for 15 min for the thermal equilibration. Subsequently, these samples were extracted or subjected to the deposition of the next layer. The inorganic multi-color EC devices fabricated in this study consist of WO_3 as the EC layer, Li_3PO_4 (LPO) as the electrolyte, WVO as the ion storage layer (i.e., EC inactive), and copper (Cu) as the current collector. The device is deposited on ITO-coated glass, and the sheet resistance is 6 Ω per square (~60 nm) with a visible light transmittance exceeding 85%. The final devices demonstrate a practical dimension of 4×4 cm^2 and possess the structure of glass/ITO/WVO/LPO/WO_3/Cu through a sequential deposition. Detailed sputtering parameters for the WO_3, Li_3PO_4, and Cu layers are listed in Table 1.

Table 1 Deposition of the WO_3, WVO, Li_3PO_4, and Cu layers.

Film	Target	Power (W)	O_2/Ar (sccm)	Pressure (Pa)
WO_3	W	120	15/45	2
Li_3PO_4	Li_3PO_4	150	5/45	2
WVO	W/V	25/165	15/45	2
Cu	Cu	120	0/50	0.5

2.2 Characterizations

Electrochemical characterizations of single and multi-layers were performed in a 1 M $LiClO_4$-PC electrolyte with a three-electrode geometry on two electrochemical workstations (CH Instruments, Inc.: CHI660E and Ivium Technologies B.V.: Ivium-N-STAT). For electrochemical measurements inside the glovebox, lithium foils served as the counter and reference electrodes in an argon-filled glovebox. For the measurement outside the glovebox, platinum foil served as the counter, and Ag/AgCl was the reference electrode.

Digital photographs of samples were taken with a Canon 850D camera. The chromaticity and reflectivity of the samples and devices are measured by a spectrophotometer (Shenzhen Threenh Technology: Benchtop Spectrophotometer TS8296). The *in-situ* optical transmission spectra under the electrochemical operations and the reflectivity of the devices were in-situ recorded by the fiber optical spectrometer (Avantes B.V.: AvaSpec-ULS2048CL-EVO).

X-ray diffraction (XRD) for structure analysis was conducted by a Rigaku Smartlab with a Cu Kα X-ray source operating at 40 kV. Multiple scans were collected between $2\theta = 10$ deg–80 deg with a scan rate of 9 deg per min. Scanning electron microscope and energy dispersive spectroscopy (SEM-EDS) for morphography element analysis was measured by Hitachi (Regulus 8230) under a voltage of 20 kV. The optical indexes were measured and fitted by an ellipsometer (J.A. Woollam Company: M-2000 ellipsometers).

3 Result and Discussion

The Bragg reflector (ITO/WVO/LPO/WO_3) plays an auxiliary function to achieve a high color saturation, and the F–P cavity (WO_3/Cu) acts as a dynamic color modulator. The combination of the Bragg reflector and F–P cavity is fundamentally oriented towards generating a focused absorption peak where the resonant center of each layer is located at the same wavelength to enhance the color contrast. Such a design is able to mitigate the irregular absorption, which could compromise the reflectance of the device across the entire visible light spectrum. Moreover, the EC inactive WVO is employed as an effective strategy to preclude the reduction of brightness and color saturation.

3.1 Electrochromism-Based F–P Cavity for Dynamic Color Modulation

By incorporating the F–P cavity, traditional transmissive EC devices can be changed to be reflective. In traditional EC devices, the transmissive mode is controlled by absorption in the EC layer to achieve color variation.[19] The varied intensity of absorption in different wavelengths leads to color variations. The F–P cavity can achieve color variation under the combined changes of refractive index and absorption. This leads to variations in the optical path difference in the cavity, thereby resulting in a reduction or enhancement of a certain wavelength range.

Inside the F–P cavity (i.e., it is WO_3/Cu in our case), the incident light repeatedly refracts, reflects, and interferes, generating coherent enhancements or subtraction. The F–P cavity can be taken as a three-layered construction consisting of layer 1 (air), layer 2 (EC layer), and layer 3 (metallic reflective layer), as shown in Fig. 1(a). The total reflectivity of F–P cavity is given as[20–22]

$$R = \frac{r_1^2 + r_2^2 + 2r_1 r_2 \cos 2\varphi}{1 + r_1^2 r_2^2 + 2r_1 r_2 \cos 2\varphi}, \tag{1}$$

where φ, $\boldsymbol{r}_1$, and $\boldsymbol{r}_2$ are expressed as

$$\varphi = \frac{2\pi}{\lambda_0} n_2 d \cos\theta_2, \tag{2}$$

$$r_1 = \frac{n_1 \cos\theta_1 - n_2 \cos\theta_2}{n_1 \cos\theta_1 + n_2 \cos\theta_2}, \tag{3}$$

$$r_2 = \frac{n_2 \cos\theta_2 - n_3 \cos\theta_3}{n_2 \cos\theta_2 + n_3 \cos\theta_3}, \tag{4}$$

where $\boldsymbol{R}$ is the total reflectivity, φ is the phase delay, $\boldsymbol{r_1}$ and $\boldsymbol{r_2}$ represent the reflection coefficients at interfaces **1** and **2**, respectively, and $\boldsymbol{d}$ is the thickness of the EC layer. $\boldsymbol{n}_i$ ($i = 1, 2, 3$) is the complex

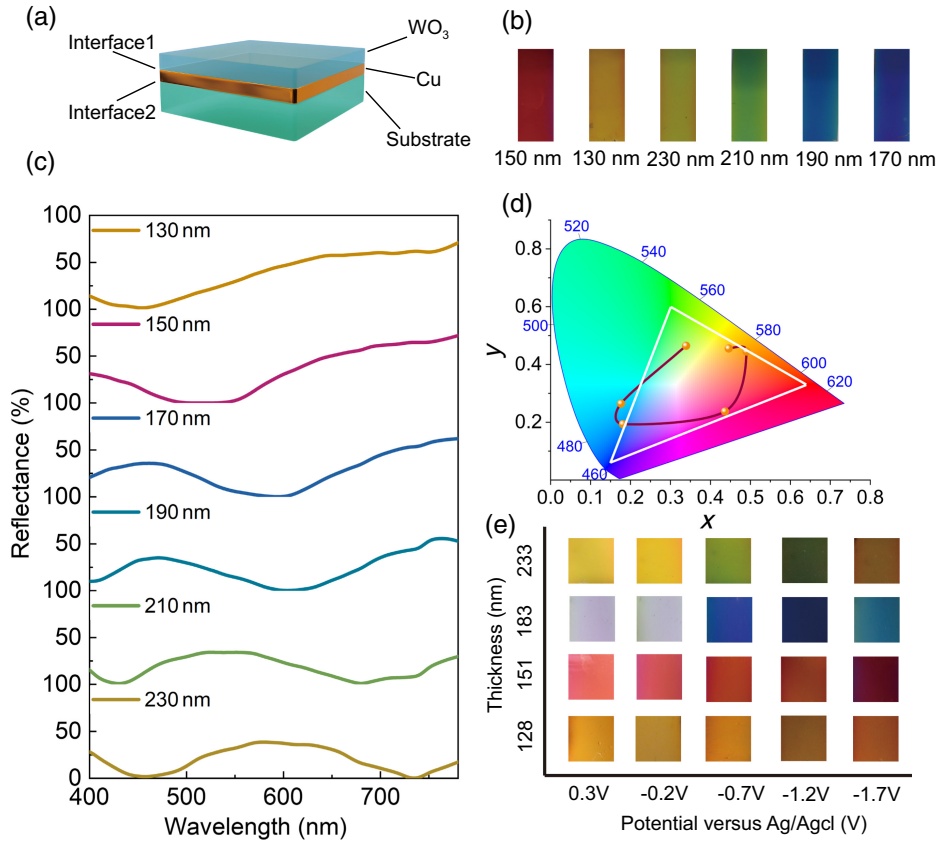

Fig. 1 Optical characterizations of the F–P cavity. (a) Schematic diagram of the F–P cavity constructed by WO_3/Cu. (b) Digital photos of the as-deposited F–P cavities with varied thicknesses of WO_3. (c) Reflectance spectrum of the F–P cavity as a function of WO_3 thickness. (d) Color coordinates for the F–P cavity with different thicknesses of WO_3. (e) Digital photos of F–P cavities working under marked potentials. The potential range was −1.7 to 0.3 V (versus Ag/AgCl) with a sweep rate of 1 mV s^{-1}.

refractive index of different layers. θ_i ($i = 1, 2, 3$) is the incident angle of each layer. According to Eq. (1), the total reflectivity is mainly determined by φ, $\boldsymbol{r_1}$, and $\boldsymbol{r_2}$. In Eq. (2), it can be seen that φ is primarily determined by $\boldsymbol{d}$ and $\boldsymbol{n}_2$. Equations (3) and (4) indicate that the reflection coefficient of each interface is determined by the complex refractive index of each layer. Hence, the thickness of the dielectric layer ($\boldsymbol{d}$) and the optical index ($\boldsymbol{n_2}$, $\boldsymbol{n_3}$) are crucial for constructing structural colors.

However, the thickness ($\boldsymbol{d}$) and the optical index ($\boldsymbol{n}, \boldsymbol{k}$) of the substrate ($\boldsymbol{n_3}$) are normally fixed once the device is fabricated. Benefiting from our employed EC material, the optical index of the EC layer can be dynamically regulated in the ion intercalation process. Therefore, the modulated optical index leads to the variation of the optical path difference and absorption. In transmissive EC devices, ion insertion commonly induces an enhancement of the absorption of a certain wavelength range by EC layers, which means that the rest of the spectra can selectively pass through. Here, the dynamic color modulation is achieved through the utilization of an EC layer with a variable refractive index in the F–P cavity, i.e., the structure of WO_3/Cu. According to Eqs. (1) and (4), the more significant the disparity between $\boldsymbol{n}_2$ and $\boldsymbol{n}_3$ is, the greater the attainable reflectance. By combining the broad absorption formed by the F–P cavity, a higher color saturation is obtained.

As mentioned, our F–P cavity constructed by the WO_3/Cu plays a core role in dynamic color modulation. This electrode is shown in Fig. 1(a), and the reflector (Cu) and dielectric layer (WO_3) are sequentially deposited on the ITO/glass. Cu was selected as the reflective layer, not only due to its significant optical mismatch with the EC layer but also due to its high reflectance of >90% beyond the wavelength of 600 nm. According to Eqs. (1) and (4), the more significant the disparity between $\boldsymbol{n}_2$ and $\boldsymbol{n}_3$ is, the greater the attainable reflectance is. By combining the

broad absorption formed via the F–P cavity, a higher color saturation is obtained. By varying the thickness of the WO_3 layer, the structural colors of magenta (red), orange, yellow, cyan (green), blue, and purple are obtained, as presented in Figs. 1(b) and 1(c). Among these colors, cyan, magenta, and yellow compose the three primary colors for the CMYK color model, and red, green, and blue comprise the tricolors for the RGB color model. In addition, the saturation of the cyan, purple, and magenta colors is beyond the sRGB color gamut, showing a very vibrant color [Fig. 1(d)]. The coordinates of the initial structural colors of six samples are revealed by modified-Bezier curves in the CIE coordinate system, demonstrating the immense potential to encompass the entire color spectrum in the F–P cavity [Fig. 1(b)]. Comparing with previous studies on WO_3/W structures,[11,12] WO_3/Cu, with varied thicknesses of the WO_3 layer, exhibits improved color saturation and brightness in forming the structural colors.

When the thickness of WO_3 is fixed at 233 nm, the color of the F–P cavity changes from the initial yellow to cyan and magenta as ions are persistently inserted [Fig. 1(e)]. The color transition is less pronounced when the thickness is relatively thin, for example, 128 and 151 nm [Fig. 1(e)]. This is due to the decreased thickness of the EC layer failing to support the substantial absorption during the ion intercalation process.[23] Moreover, it is discernible that the reflectivity decreases with increasing the thickness of WO_3, whereas the quantity of absorption peaks demonstrates a proportional escalation with increasing the thickness. The interference of the lower order primarily occurs with a thickness of about $\boldsymbol{m}_{\text{low}} \cdot \lambda/4\boldsymbol{n}_2$ (where $\boldsymbol{m}_{\text{low}} = 1$). When the thickness is relatively thick $\boldsymbol{m}_{\text{high}} \cdot \lambda/4\boldsymbol{n}_2$ (where $\boldsymbol{m}_{\text{high}}$ is an odd number greater than 1), a higher-order interference immediately emerges in the spectrum. The number of absorption peaks in the spectrum gradually increases with the increase of the interference order, eventually yielding a low reflectance. This tendency can also be observed in the reflectance spectrum in that the absorption was split from a single-peak to a double-peak in the range of 130 to 230 nm [Fig. 1(c)]. Thus, the thickness should be appropriately selected in the potential device to balance the brightness of the structural color and the color variation range.

3.2 Design for Focused Bragg Reflection

The Bragg reflector, a quarter-wave stack with a one-dimensional array in high and low refractive indexes, is strategically employed to construct the initial structural color. The Bragg reflector is constructed by the current collector (ITO), ion storage electrode (WVO), electrolyte (Li_3PO_4), and EC layer (WO_3), all of which contribute to the high saturation in a quarter-wave stack. The reflectance peaks of the Bragg reflector can be varied according to thickness and variation of refractive indexes. The reflector was stacked based on the periodic laws of high and low refractive indexes interleave, and the parameters are described by the following equations:[22,24]

$$\lambda_B = \frac{2(n_L d_L + n_H d_H)}{m}, \tag{5}$$

$$R = \left(\frac{n_o - n_s \left(\frac{n_H}{n_L}\right)^{2N}}{n_o + n_s \left(\frac{n_H}{n_L}\right)^{2N}} \right)^2, \tag{6}$$

$$\Delta E = \frac{4}{\pi} E \frac{|n_H - n_L|}{n_H + n_L}, \quad E = \frac{hc}{\lambda_B} = \frac{1240}{\lambda_B} \text{ eV}, \tag{7}$$

where λ_B is the central wavelength of the Bragg reflector in the reflectivity spectrum. $\boldsymbol{m}$ represents the diffraction order. $\boldsymbol{N}$ is the number of bilayers. $\boldsymbol{n}_L$ and $\boldsymbol{n}_H$ are the low and high refractive indexes, respectively. $\boldsymbol{d}_L$ and $\boldsymbol{d}_H$ are the thicknesses of the materials of low and high refractive indexes, respectively. $\boldsymbol{n}_o$ and $\boldsymbol{n}_s$ represent the refractive indexes of the incident light and the substrate, respectively. In brief, with the larger number of bilayers ($\boldsymbol{N}$) and the difference between $\boldsymbol{n}_L$ and $\boldsymbol{n}_H$ being more significant, the reflectivity of the Bragg reflector becomes higher. The severe mismatch between the high and low refractive index of the Bragg reflector can realize higher reflectivity. As a result, such an apparent mismatch induces a higher initial color saturation of the device.

According to Eq. (6), the arrangement of high and low refractive index layers is designed. The refractive indexes ($\boldsymbol{n}$) of ITO, WVO, and WO_3 are around 2.0, which are categorized as high

Table 2 Measured refractive index and thickness of each layer.

Material	Refractivity index (n) @600 nm	Thickness (d)
ITO	1.89	~110 nm
WVO	1.99	~110 nm
Li_3PO_4	1.57	~280 nm
WO_3	2.04	~220 nm

refractive index parts. By contrast, LPO, with a refractive index close to 1.5, is selected as the low refractive index layer. The detailed parameters of the reflective layers are listed in Table 2. This leads to a refractive index mismatch at the interface of the high and low refractive layers. According to Eqs. (6) and (7), a more substantial distinction between $\boldsymbol{n}_L$ and $\boldsymbol{n}_H$ indicates a more pronounced mismatch. Therefore, a stacking approach with refractive indexes of approximately 2 and 1.5 is designed to form structural colors. It is worth noticing that the stacking number $\boldsymbol{N}$ in Eq. (6) determines the intensity of the reflection peaks: a more considerable $\boldsymbol{N}$ results in a sharper peak, which implies a higher contrast. However, considering the sandwich structure of an EC device, we determined the number of reflective layers at 3 for the EC layer, electrolyte, and counter electrode, respectively.

The correlation between the stacked functional layers and the quarter-wave can be validated from the experiments, as discussed below. The center wavelength of the Bragg reflector was determined based on Eq. (5), and the reflectivity was simulated with the assistance of the finite-difference time-domain method (FDTD). The thickness of each layer is fixed by aligning their refractive indexes. We demonstrate a Bragg reflector with a center wavelength of 600 nm as a representative. The refractive index and thickness of each layer are shown in Table 2, where a series of thicknesses are strictly controlled to follow a quarter-wave format. According to this design, the construction of the Bragg reflector (ITO/WVO/LPO/WO_3) was deposited layer by layer [Fig. 2(a)]. Primarily, the ITO-coated glass is transparent, and the WVO layer on ITO presents a light green color with a broad peak in the reflectance spectrum [Fig. 2(c)]. According to Eq. (2), the formation of broad reflection peaks is limited by the number of stacked layers, and the intensity of the reflection peak gradually increases with the number of stacking bilayers [Figs. 2(c) and 2(d)]. The initial green structural color gradually switches to yellow along with an increase in the number of stacked layers, as shown in the CIE coordinate in Fig. 2(b). Moreover, the optical indexes ($\boldsymbol{n}$ and $\boldsymbol{k}$) in the visible spectra used in our optical simulation are shown in Figs. 2(e) and 2(f).

3.3 Counter Elelctrode Selection

Traditional EC devices typically present a low reflectance or transmittance due to the simultaneous absorption of the two EC electrodes upon ion intercalation. By contrast, in devices consisting of a F–P cavity, the color variation is primarily achieved by altering the optical index of the EC layer during the EC process. To avoid excessive and non-gain absorption, we choose to employ an EC inactive material (WVO)[25] as the counter electrode.

The WVO film is co-sputtered from the pure W and V targets in the mixed atmosphere of Ar and O_2. Its primary atomic ratio of W : V is 46.08 : 53.92 characterized by SEM-EDS, close to 1:1. Only the diffraction peaks from ITO were identified for the deposited WVO films on ITO/glass [Fig. 3(a)], indicating an amorphous nature of the as-deposited WVO films. The transmittance of WVO exceeds those of WO_3 and V_2O_5 beyond the 500 nm wavelength [Fig. 3(b)], and the extinction coefficient ($\boldsymbol{k}$) of WVO is almost zero as the wavelength is beyond 450 nm [Fig. 3(c)]. The high transmittance and low extinction coefficient enable the reduction of the negative optical impact, and it can therefore eliminate the influence on the reflectance in an assembled device. Compared with the light blue (WO_3) and yellow (V_2O_5), the WVO exhibits a light green color that is stretched from the two colors and is close to the origin (i.e., the white point) in the CIE color space [Fig. 3(d)]. All figure-of-merits of WVO play a positive role for improving the brightness and saturation. Hence, the neutral light green colors are more suitable for the devices.

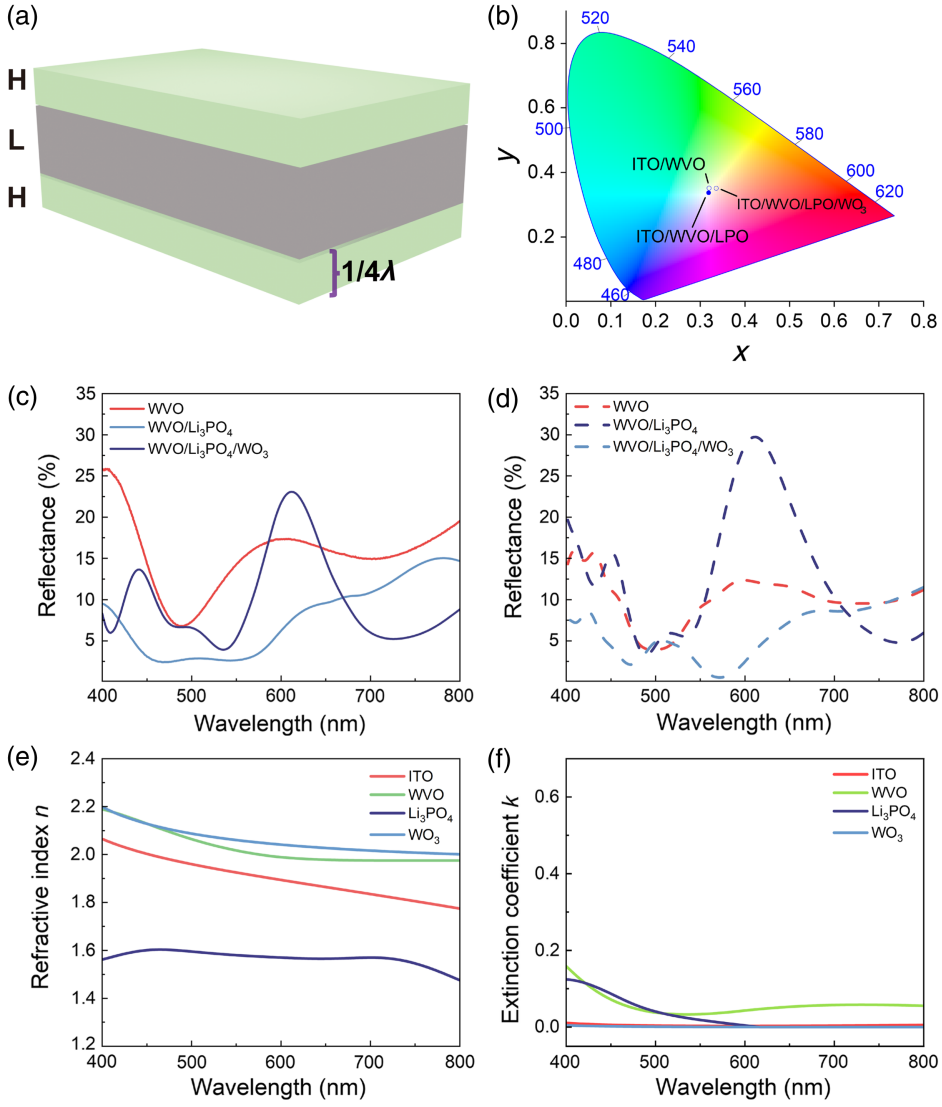

Fig. 2 Bragg reflector design. (a) Schematic diagram of our Bragg reflector (ITO/WVO/LPO/WO_3), with ***H*** and ***L*** representing the high and low refractive indexes, respectively. (b) Color coordinates for the monolayer of WVO, WVO/LPO, and WVO/LPO/WO_3 in CIE 1931 color space. (c) and (d) The reflectance of WVO, WVO/LPO, and WVO/LPO/WO_3 from experiments and simulations. The solid line and dashed line represent the experiments and the simulations data, respectively. (e) and (f) The refractive index and extinction coefficient of ITO, WVO, Li_3PO_4, and WO_3 in the visible range.

The WVO films were subjected to cyclic voltammetry in the potential window of 2.0 to 4.0 V versus Li/Li^+, and the results showed a maximum charge capacity of 22.5 mC cm^{-2} [Fig. 3(e)] and nearly a non-variation of the optical spectra [i.e., EC in-active, Fig. 3(f)]. The obtained charge capacity of WVO matched well with amorphous WO_3 (~20 mC cm^{-2})[26] in the same potential range, enabling mutual charge balancing and stable potential windows for ion intercalation. The non-regulation in the spectra also proves that the operation of the WVO film itself rarely alters the optical modulation of a device.

3.4 Full EC Device Demonstration

Finally, an all-solid-state EC device based on the combination of the Bragg reflector and F–P cavity was fabricated. The structure of the device is illustrated in Fig. 4(a), which is composed of glass/ITO/WVO/LPO/WO_3/Cu. The device can be considered as two optical stacks: a Bragg reflector consisting of ITO/WVO/LPO/WO_3 and an F–P cavity formed by WO_3/Cu.

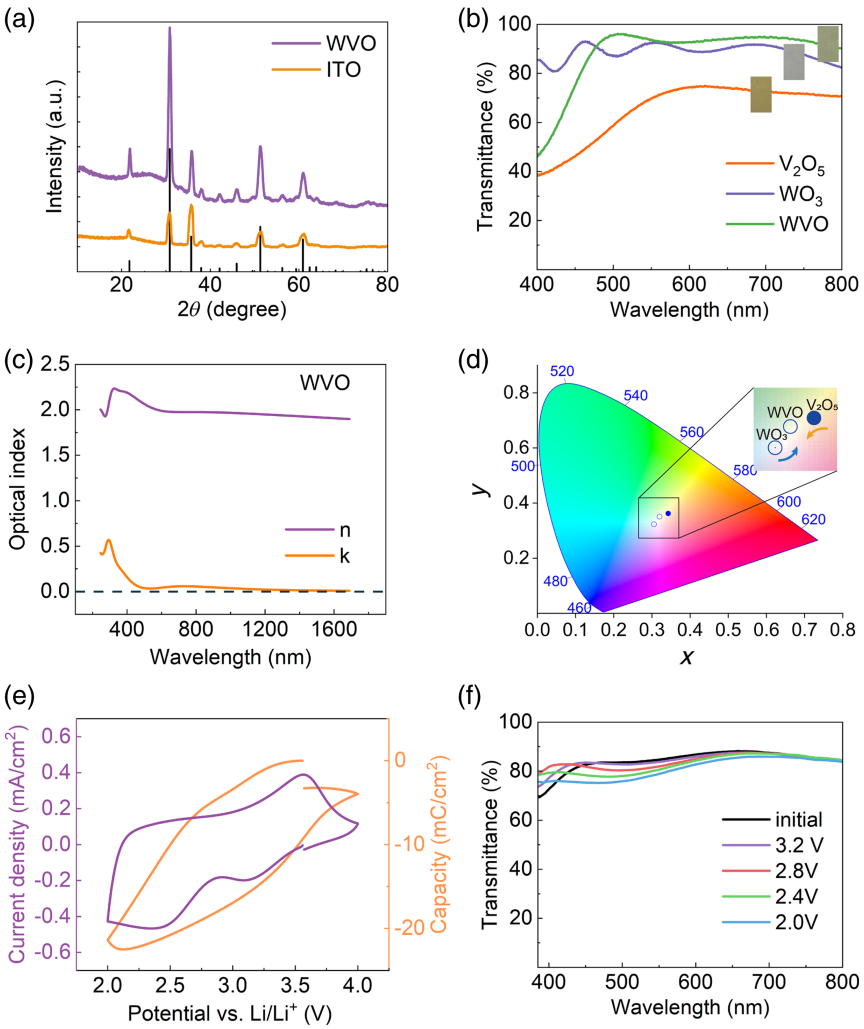

Fig. 3 Characterizations of mixed-tungsten-vanadium oxide (WVO). (a) XRD patterns of the WVO layer on ITO/glass (the black vertical line is the label of PDF#97-005-0848 for crystal ITO). (b) The reflectance of WO_3, V_2O_5, and WVO. (c) Optical index of the WVO film. (d) Color coordinates for WO_3, V_2O_5, and WVO. (e) Cyclic voltammetry curve of the WVO film. (f) The *in-situ* transmittance variation of the WVO film upon the CV cycle in the range of 2.0 to 4.0 V (versus Li/Li^+) with a sweep rate of 20 mV s^{-1}.

The formed structural colors are facilitated by the designed Bragg reflection. All reflection peaks were focused at the designed wavelength (~600 nm) in the reflective device, resulting in a uniform absorption in the device that is beneficial for achieving color purity. Meanwhile, the F–P cavity primarily undertakes the function of color variation. By incorporating of EC material (WO_3), the reflector with a fixed structure enables the transition from static structural colors to dynamic color modulation in the solid-state EC device. Based on the aforementioned experiments and FDTD simulations in Figs. 2(c) and 2(d), the thickness of each layer is fixed [Fig. 4(a)] to yield a center absorption wavelength at 600 nm of the EC device for demonstration. The direction of the color shift and its position in the CIE space are illustrated in Fig. 4(b), transitioning from an initial grass-green to the dark brown [Fig. 4(c)]. So far, the limited magnitude of this transition is attributed to the constraints of solid/solid interface during the fabrication process; for example, the ion intercalation between WO_3 and LPO is insufficient for varying the optical constants in WO_3 due to poor interface contact. We believe that the desired outcome can be achieved by improving the fabrication in the future. However, a high reflectance (37%) in the device [Fig. 4(c)] was still maintained due to the utilization of the WVO electrode and our optical stacking strategies. The color difference (ΔE^*_{ab}) is utilized to quantify the degree of color variation.

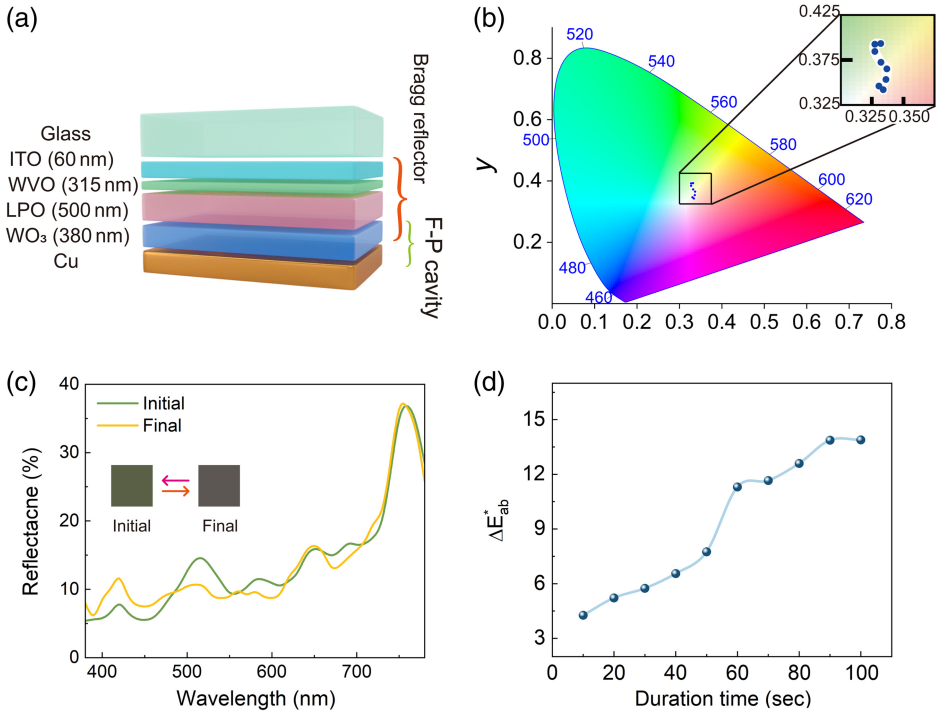

Fig. 4 Optical performance of the solid-state EC device. (a) Schematic diagram of the device structure composed of a Bragg reflector and an F–P cavity. (b) The dynamic transition of color coordinates in the 1931 CIE color space upon ion intercalation. (c) The reflectance in the visible range of the device. Inset: digital photos of the color variation. (d) Variation of the color difference under the external electric field (−2 V) in different duration times.

ΔE^*_{ab} is the separation between two colors and can quantify the small change of color variation. It is described in CIE coordinates of L, a, and b (termed as CIELAB) as[27]

$$\Delta E^*_{ab} = \sqrt{\Delta L^2 + \Delta a^2 + \Delta b^2}, \tag{8}$$

where ΔL is the difference between the initial and final values corresponding to perceptual lightness and a and b control the red-green and yellow-blue in CIELAB color space, respectively. Δa and Δb are the difference values of "a" and "b" between the initial and final in CIELAB color space, respectively. When the value of ΔE^*_{ab} exceeds approximately 2.3, it can be captured by human eyes.[28,29] Our device ultimately achieved the maximum color difference (ΔE^*_{ab}) of 13.8 at a voltage of −2 V for 100 s [Fig. 4(d)].

To clarify the difference between the traditional device and our current design, we performed FDTD simulations. First, when the multilayer stacking is a random selection of the material and its thickness (i.e., traditional design), for example, ITO(300 nm)/NiO(400 nm)/$LiNbO_3$(200 nm)/WO_3(500 nm)/Al(300 nm), as shown in Fig. 5(a), the irregular arrangement of refractive indexes and the arbitrary thickness design cause a discord resonance. Thus the structural color is hard to form, as revealed by the redundant interference fringe in the reflectance spectrum [Fig. 5(c)]. Such a chaotic optical stacking causes irregular enhancement and extinction, which hinders the reflection of an object from showing a pure color. By combining the Bragg reflector and the F–P cavity design into the device, optical interference can be taken as an effective approach for reflective EC devices to form the multicolor variation. This Bragg reflector is designed according to the alternating arrangement rule of high and low refractive indexes, and the thickness of each layer strictly coincides with the quarter-wave, with the primary objective of attaining consistent optical enhancement or suppression. This deliberate design seeks to optimize color saturation while circumventing irregular interference, which could otherwise lead to a reduction in the reflectance characteristics of the reflector. The configuration of ITO(65 nm)/WVO(105 nm)/Li_3PO_4(220 nm)/WO_3(170 nm)/Al(300 nm) was taken as

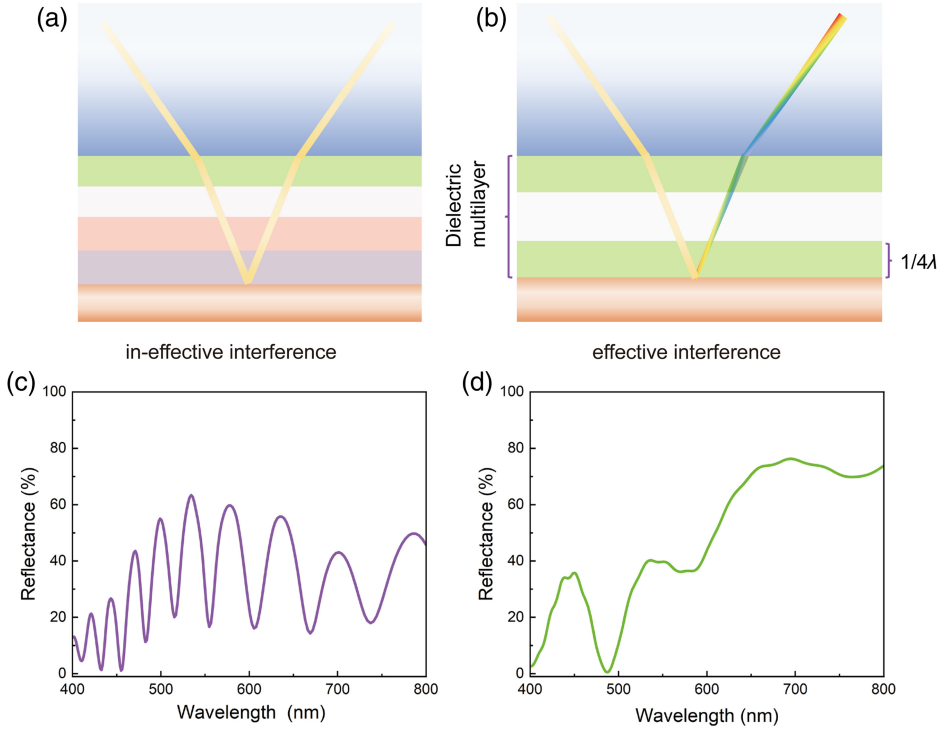

Fig. 5 Structural design for the traditional device and our device combined of the Bragg reflector and the F–P cavity. (a) and (b) Schematic diagram of the traditional device and our device. (c) and (d) Simulated the reflectivity of the traditional device and our device.

our example [Fig. 5(b)], by carefully selecting the material of each layer and its thickness. In this device combining the Bragg reflector and F–P cavity, the resonance absorption peak was designed at 500 nm, showing a remarkable orientation in color [Fig. 5(d)].

4 Conclusion

We designed structural color and dynamic color variation by combining the Bragg reflector and F–P cavity. The Bragg reflector plays an auxiliary role in the initial structural colors and subsequent dynamic color regulation. The F–P cavity possesses an initial color and can dynamically vary the colors in the ion intercalation process by effectively regulating the optical index of the EC material (WO_3). To sum, by combining the Bragg reflector and the F–P cavity through the optical stacking, the construction of initial structural colors and the subsequent dynamic regulation is demonstrated to be effective. Although the dynamic modulation range of current EC devices is limited, it is possible to fabricate devices with high brightness, high color saturation, and extensive modulation range by identifying the optimal fabrication parameters. All layers with inorganic materials in the device can be fabricated by magnetron sputtering; therefore, a stable performance can be anticipated from the layers to the device level.

In addition, the EC and ion storage electrode are the core of the device for conventional EC designs. Extensive work[9,10,12,30–33] has been devoted to designing the working electrodes in EC devices. However, the selection of counter electrodes is rarely considered. In this work, we employed EC inactive WVO as a counter electrode, which can ensure high reflectivity and contrast of the device. We believe that the optical stacking approach will become a potential solution for various multifunctional devices using optical cavities, such as thermochromic, photochromic, and photoluminescent technologies. Other display technologies, such as laser technology and optical sensors, can also be implemented through optical stacking to extend the functionalities.

Disclosures

The authors declare no competing interests.

Code and Data Availability

All data in support of the findings of this paper are available within the article.

Acknowledgments

This work was financially supported by the "Shenzhen Science and Technology Innovation Commission" (Grant Nos. 20220815095607001 and JCYJ20210324105402007), National Natural Science Foundation of China (Grant No. 52172294), Guangdong Provincial Innovation and Entrepreneurship Project (Grant No. 2017ZT07C071), National Natural Science Foundation of Guangdong (Grant No. 4685326), Guangdong-Hong Kong-Macau Joint Laboratory on Micro-Nano Manufacturing Technology (Grant No. 2021LSYS004), and Guangdong Provincial Key Laboratory Program (Grant No. 2021B1212040001) from the Department of Science and Technology of Guangdong Province. The film deposition work used the resources from SUSTech Core Research Facilities that receives support from the Shenzhen Municipality.

References

1. W. Wu et al., "Temperature-dependent electrochromic devices for energy-saving dual-mode displays," *ACS Appl. Mater. Interfaces* **15**(3), 4113–4121 (2023).
2. A. Llordés et al., "Tunable near-infrared and visible-light transmittance in nanocrystal-in-glass composites," *Nature* **500**(7462), 323–326 (2013).
3. C. G. Granqvist, "Oxide electrochromics: an introduction to devices and materials," *Sol. Energy Mater. Sol. C* **99**, 1–13 (2012).
4. C. Sui and P.-C. Hsu, "Radiative electrochromism for energy-efficient buildings," *Nat. Sustain.* **6**, 428–437 (2023).
5. C. Sui et al., "Dynamic electrochromism for all-season radiative thermoregulation," *Nat. Sustain.* **6**(4), 428–437 (2023).
6. Q. Huang et al., "Recent progress in transmissive and reflective electrochromic devices for multi-color modulation," *Sol. Energy Mater. Sol. C* **267**, 112706 (2024).
7. X. Wang, N. Miura, and N. Yamazoe, "Study of WO_3-based sensing materials for NH_3 and NO detection," *Sens. Actuators B: Chem.* **66**(1–3), 74–76 (2000).
8. J. A. Dirksen, K. Duval, and T. A. Ring, "NiO thin-film formaldehyde gas sensor," *Sens. Actuators B: Chem.* **80**(2), 106–115 (2001).
9. E. Redel et al., "Electrochromic Bragg mirror: ECBM," *Adv. Mater.* **24**(35), 265–269 (2012).
10. L. Xiao et al., "WO_3-based electrochromic distributed Bragg reflector: toward electrically tunable microcavity luminescent device," *Adv. Opt. Mater.* **6**(1), 1700791 (2018).
11. J. Chen et al., "Fabry-Perot cavity-type electrochromic supercapacitors with exceptionally versatile color tunability," *Nano Lett.* **20**(3), 1915–1922 (2020).
12. Z. Wang et al., "Towards full-colour tunability of inorganic electrochromic devices using ultracompact Fabry-Perot nanocavities," *Nat. Commun.* **11**(1), 302 (2020).
13. A. Chaudhary et al., "Prussian blue-cobalt oxide double layer for efficient all-inorganic multicolor electrochromic device," *ACS Appl. Electron. Mater.* **2**(6), 1768–1773 (2020).
14. M. ElKabbash et al., "Fano-resonant ultrathin film optical coatings," *Nat. Nanotechnol.* **16**(4), 440–446 (2021).
15. M. ElKabbash et al., "Fano resonant optical coatings platform for full gamut and high purity structural colors," *Nat. Commun.* **14**(1), 3960 (2023).
16. O. A. M. Abdelraouf et al., "All-optical switching of structural color with a Fabry–Pérot cavity," *Adv. Photonics Res.* **4**(11), 2300209 (2023).
17. Y. Liu et al., "Structural color three-dimensional printing by shrinking photonic crystals," *Nat. Commun.* **10**(1), 4340 (2019).
18. P. Hosseini, C. D. Wright, and H. Bhaskaran, "An optoelectronic framework enabled by low-dimensional phase-change films," *Nature* **511**(7508), 206–211 (2014).
19. C. G. Granqvist, *Handbook of Inorganic Electrochromic Materials*, Elsevier (1995).
20. O. S. Heavens, *Optical Properties of Thin Solid Films*, Courier Corporation (1991).
21. M. Born and E. Wolf, *Principles of Optics: Electromagnetic Theory of Propagation, Interference and Diffraction of Light*, Elsevier (2013).
22. H. A. Macleod, *Thin-film Optical Filters*, CRC Press (2017).
23. B. W.-C. Au, K.-Y. Chan, and D. Knipp, "Effect of film thickness on electrochromic performance of sol-gel deposited tungsten oxide (WO3)," *Opt. Mater.* **94**, 387–392 (2019).
24. L. Liu et al., "Electrochromic photonic crystal displays with versatile color tunability," *Electrochem. Commun.* **13**(11), 1163–1165 (2011).
25. J. Wang et al., "Amorphous mixed-vanadium-tungsten oxide films as optically passive ion storage materials for solid-state near-infrared electrochromic devices," *ACS Appl. Mater. Interfaces* **15**(5), 7120–7128 (2023).

26. R.-T. Wen, C. G. Granqvist, and G. A. Niklasson, "Eliminating degradation and uncovering ion-trapping dynamics in electrochromic WO_3 thin films," *Nat. Mater.* **14**(10), 996–1001 (2015).
27. A. R. Robertson, "The CIE 1976 color-difference formulae," *Color Res. Appl.* **2**(1), 7–11 (1977).
28. M. Melgosa, J. J. Quesada, and E. Hita, "Uniformity of some recent color metrics tested with an accurate color-difference tolerance dataset," *Appl. Opt.* **33**(34), 8069–8077 (1994).
29. G. Sharma and R. Bala, *Digital Color Imaging Handbook*, CRC Press (2017).
30. Q. Zhang et al., "Preparation of a $Pb@SiO_2$ photonic crystal composite with enhanced electrochromic performance," *ACS Appl. Electron. Mater.* **3**(10), 4441–4447 (2021).
31. B. Wang et al., "A facile strategy to construct $Au@V_xO_{2x+1}$ nanoflowers as a multicolor electrochromic material for adaptive camouflage," *Nano Lett.* **22**(9), 3713–3720 (2022).
32. Y. Li et al., "Dynamic tuning of gap plasmon resonances using a solid-state electrochromic device," *Nano Lett.* **19**(11), 7988–7995 (2019).
33. E. Hopmann and A. Y. Elezzabi, "Plasmochromic nanocavity dynamic light color switching," *Nano Lett.* **20**(3), 1876–1882 (2020).

Rui-Tao Wen is currently an associate professor in the Department of Materials Science and Engineering at SUSTech. He earned his PhD from Ångströmlaboratoriet at Uppsala University, Sweden, in 2016 and carried out postdoc work at Massachusetts Institute of Technology, United States, before joining SUSTech. His research interests include electrochromic devices, epitaxy growth of semiconductor materials for electric, and photonic applications.

Biographies of the other authors are not available.